Ontogeny of Cone Photoreceptor Mosaics in Zebrafish

W. Ted Allison,[1]* Linda K. Barthel,[2] Kristina M. Skebo,[1] Masaki Takechi,[3] Shoji Kawamura,[3] and Pamela A. Raymond[2]

[1]Departments of Biological Sciences and Medical Genetics, University of Alberta, Edmonton, Alberta, Canada T6G 2E9
[2]Department of Molecular, Cellular, and Developmental Biology, University of Michigan, Ann Arbor, Michigan 48109
[3]Department of Integrated Biosciences, Graduate School of Frontier Sciences, University of Tokyo, Kashiwa, Chiba 277-8562, Japan

ABSTRACT

Cone photoreceptors in fish are typically arranged into a precise, reiterated pattern known as a "cone mosaic." Cone mosaic patterns can vary in different fish species and in response to changes in habitat, yet their function and the mechanisms of their development remain speculative. Zebrafish (*Danio rerio*) have four cone subtypes arranged into precise rows in the adult retina. Here we describe larval zebrafish cone patterns and investigate a previously unrecognized transition between larval and adult cone mosaic patterns. Cone positions were determined in transgenic zebrafish expressing green fluorescent protein (GFP) in their UV-sensitive cones, by the use of multiplex in situ hybridization labelling of various cone opsins. We developed a "mosaic metric" statistical tool to measure local cone order. We found that ratios of the various cone subtypes in larval and adult zebrafish were statistically different. The cone photoreceptors in larvae form a regular heterotypic mosaic array; i.e., the position of any one cone spectral subtype relative to the other cone subtypes is statistically different from random. However, the cone spectral subtypes in larval zebrafish are not arranged in continuous rows as in the adult. We used cell birth dating to show that the larval cone mosaic pattern remains as a distinct region within the adult retina and does not reorganize into the adult row pattern. In addition, the abundance of cone subtypes relative to other subtypes is different in this larval remnant compared with that of larvae or canonical adult zebrafish retina. These observations provide baseline data for understanding the development of cone mosaics via comparative analysis of larval and adult cone development in a model species. J. Comp. Neurol. 518:4182–4195, 2010.

INDEXING TERMS: heterotypic cell mosaic; row mosaic; metamorphosis; opsin; multiplex in situ hybridization; teleost

Homotypic mosaics of cells, in which the spatial arrangement of cells of a given type is regular, are common in multicellular organisms. Examples include the equal spacing of bird feathers on the skin and the distribution of photoreceptors and other types of neurons in the retina (Cameron and Carney, 2004; Eglen et al., 2003; Reese et al., 2005; Tyler and Cameron, 2007). Heterotypic arrangements of cells, in which different cell types are arranged in a pattern relative to each other that is statistically different from random (e.g., different types of photoreceptors within fly ommatidia), are not as readily observable in vertebrates (Eglen and Wong, 2008). Arguably, the importance of spatial relationships among heterotypic cell types in the vertebrate central nervous system has been underappreciated; likely roles include both proper neuron differentiation and functional connectivity (Eglen and Galli-Resta, 2006; Eglen et al., 2008; Fuerst et al., 2008). The cone photoreceptor mosaics in teleost fish represent a uniquely accessible example of vertebrate heterotypic neuronal mosaics.

Additional Supporting Information may be found in the online version of this article.

Grant sponsor: National Institutes of Health; Grant number: R01 EY015509 (to P.A.R.); Grant sponsor: Natural Sciences and Engineering Research Council of Canada (to W.T.A.).

*CORRESPONDENCE TO: W. Ted Allison, Departments of Biological Science and Medical Genetics, University of Alberta, Edmonton, Alberta, Canada T6G 2E9. E-mail: ted.allison@ualberta.ca

Received July 25, 2009; Revised May 9, 2009; Accepted June 1, 2010
DOI 10.1002/cne.22447
Published online June 17, 2010 in Wiley Online Library (wileyonlinelibrary.com)

Cone photoreceptors in teleost fish are similar to those of other vertebrates, with multiple subtypes varying in their spectral sensitivity as a result of the differential expression of opsin genes. The differing spectral sensitivities of individual cones underpin color vision (Risner et al., 2006). One of the striking features of teleost cone photoreceptors that differentiates them from those of other vertebrates is their spatial arrangement into regular, heterotypic mosaics: reiterated patterns of cone spectral subtypes precisely arranged relative to one another across the retina. Different teleost species have variations on this mosaic pattern (Ali and Anctil, 1976; Collin, 2008; Collin and Shand, 2003), generally categorized as row and square mosaics, in which double and single cone photoreceptors are arranged in parallel rows or in a lattice arrangement of squares, respectively. Some species appear to transition between row and square mosaics during ontogeny (Lyall, 1957; Shand et al., 1999), and several other variations on the mosaic geometry have been identified (Ali and Anctil, 1976; Collin, 2008). Hypotheses addressing the adaptive value (Collin, 2008) and developmental mechanisms (Raymond and Barthel, 2004) of the cone mosaic have been proposed but not experimentally tested. The only other group of vertebrates for which a heterotypic cone mosaic has been described are certain species of diurnal geckos (Cook and Noden, 1998; Dunn, 1966).

Among teleost species investigated (Engström, 1960, 1963), the row mosaic in zebrafish, *Danio rerio*, is one of the most precise in its arrangement of cones, with photoreceptors rarely out of register with the pattern. Zebrafish possess four cone spectral subtypes: ultraviolet (UV)-, blue-, green-, and red-sensitive cones that express *SWS1* (also known as *opn1sw1*), *SWS2* (also known as *opn1sw2*), *RH2* (also known as *opn1mw1, opn1mw2, opn1mw3, opn1mw4*), or *LWS* (also known as *opn1lw1, opn1lw2*) cone opsin genes, respectively (Allison et al., 2004; Cameron, 2002; Chinen et al., 2003; Raymond et al., 1993, 1996; Vihtelic et al., 1999). This stereotyped pattern of cones (see Fig. 1) includes a fixed ratio of cones from each subtype, wherein red- or green-sensitive cones occur twice as often as UV- or blue-sensitive cones. Rows of red-/green-sensitive double cone pairs alternate with rows of blue- and UV-sensitive single cones, and these cone rows radiate outward as meridians orthogonal to the retinal perimeter. The morphology of this mosaic has been established by using histology (Engström, 1960), and the identity of the cone subtypes has been established through opsin gene expression analysis (Raymond et al., 1993, 1996; Takechi and Kawamura, 2005), through opsin immunohistochemistry (Vihtelic et al., 1999), and by matching cone morphology to spectral absorbance measured by microspectrophotometry (Allison et al., 2004; Cameron, 2002; Nawrocki et al., 1985; Robinson et al., 1993).

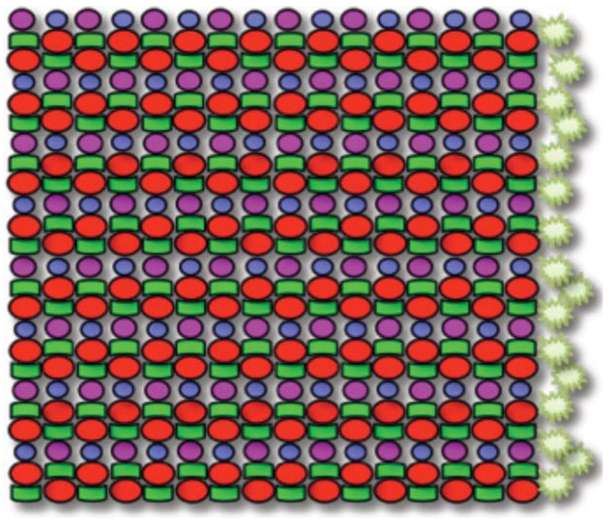

Figure 1. Schematic of the planar mosaic arrangement of cone photoreceptors in zebrafish: a heterotypic mosaic of cone subtypes organized in a precise, reiterated row pattern. Four cone photoreceptor subtypes are present, including UV (magenta), B (blue), G (green), and R (red), in a precise ratio: twice as many R or G cones relative to UV or B cones, equal numbers of R and G cones, and equal numbers of B and UV cones. The spatial arrangement is highly stereotyped, with alternating rows of R/G double cones and B/UV single cones. The starbursts represent proliferating cells that give rise to new cone photoreceptors throughout the life of the fish in the marginal germinal zone, an annulus orthogonal to the cone rows, and at the boundary between neural retina and ciliary epithelium. [Color figure can be viewed in the online issue, which is available at wileyonlinelibrary.com.]

In this study we used zebrafish as a model to gain insights into formation of the vertebrate cone mosaic. Because the retina of teleosts continues to grow by addition of new cells throughout the life of the fish, some developmental mechanism must also allow the pattern and/or identity of differentiating cones to be continuously replicated (Raymond and Barthel, 2004). Addition of new cells at the retinal periphery is analogous to addition of rings on a tree; thus, when viewed in flat mount, retina that was generated in the embryo and larva is in the center of the retina near the optic nerve head, whereas more recently generated retina is toward the tissue periphery (the outermost "rings"). We anticipate that the specification of cone identity and position are closely intertwined, consistent with the spatiotemporal relationship of cone differentiation and selective expression of opsin genes (Stenkamp et al., 1996, 1997). Zebrafish are a premier genetic and developmental model for understanding both cone mosaic formation (Cameron and Carney, 2000; Raymond and Barthel, 2004; Raymond and Hitchcock, 2004; Stenkamp and Cameron,

2002) and vertebrate cone subtype specification/differentiation (Adler and Raymond, 2008; Takechi et al., 2008).

Here we report our observation that all spectral subtypes of cone photoreceptors in larval zebrafish are distributed in a regular heterotypic mosaic, but the precise row mosaic pattern of adult fish is lacking; furthermore, the ratio of cone spectral subtypes in the larva differs from that in the adult retina. We then asked whether the cone photoreceptors generated during larval development later reorganize into the adult row mosaic or instead retain the larval pattern. Our analyses using birth-dating techniques to identify the larval photoreceptors showed that the latter was true; i.e., the remnant of larval retina in the adult fish retains the less well-organized mosaic pattern characteristic of the larval retina. Our observations provide a unique opportunity to examine mechanisms of heterotypic mosaic formation through comparing ontogenetic stages within the zebrafish model organism.

MATERIALS AND METHODS

Animal care and use

Zebrafish (*Danio rerio*) were raised and maintained using standard protocols (Westerfield, 1995) in E3 media and aquaria system water at 28.5°C with or without PTU (1-phenyl-2-thiourea) to block formation of melanin pigment. Most experiments used transgenic zebrafish Tg(*-5.5opn1sw1:EGFP*)*kj9* expressing GFP in the UV cones, driven by the SWS1 opsin (ZFin ID: ZDB-GENE-991109-25) promoter in a WIK genetic background (Takechi et al., 2003). To isolate neural retina in adults, the fish were dark-adapted overnight, and the neural retina was dissected away from other ocular tissues and fixed in 4% paraformaldehyde with 5% sucrose in phosphate-buffered saline (pH 7.4). To visualize larval retina, fish at 3 or 4 days postfertilization (dpf) were fixed in this same fixative and dissected to remove lenses, and eyes were mounted to visualize cones through the sclera. Tissues were mounted in a glycerol-based p-phenylenediamine antifade medium (Johnson and Araujo, 1981). All procedures were approved by the Use and Care of Animals in Research Committee at the University of Michigan.

Cell birth dating

Thymidine analogs 5-bromo-2′-deoxyuridine (BrdU; Sigma-Aldrich, St. Louis, MO; No. B5002) and/or 5-iodo-2′-deoxyuridine (IdU; MP Biochemicals, Solon, OH; No. 100537) were diluted in E3 media at 10 mM, and fish were maintained in this water overnight at 28.5°C (Westerfield, 1995). BrdU was detected by using rat anti-BrdU antibody (raised against BrdU; Accurate Chemical, Westbury, NY; No. OBT0030S; diluted 1:50) that labels BrdU (but not IdU) and/or mouse anti-BrdU (raised against BrdU; BD Pharmingen, San Diego, CA; No. 555627; diluted 1:50) that labels both BrdU and IdU (Vega and Peterson, 2005). These antibodies failed to label the retina if BrdU or IdU was not applied to the animal (data not shown). Immunohistochemistry was performed on isolated, flat-mounted neural retinas. A blocking step consisted of incubating retinas in 10% normal goat serum diluted in phosphate-buffered saline containing 1% Tween 20, 1% Triton X-100, and 1% dimethyl sulfoxide at pH 7.2 (PBS-TTD). Antibodies were diluted in 2% heat-inactivated goat serum diluted in PBS-TTD. Secondary antibodies were anti-mouse and anti-rat conjugated to AlexaFluor fluorochromes 488, 568, or 647 (Invitrogen, Carlsbad, CA) diluted in the same buffer at 1:1,000. In some cases, the detection of BrdU and/or IdU was carried out following in situ hybridization with labeled cone opsin riboprobes, including an antigen retrieval step with 2 N HCl for 30 minutes.

Multiplex in situ hybridization to detect cone positions

The localization of blue-, green-, and red-sensitive cones (B, G, and R cones, respectively) used previously characterized (Raymond and Barthel, 2004; Takechi and Kawamura, 2005) in situ hybridization riboprobes against appropriate opsins, in combination with multiplex fluorescent detection technology. To ensure detection of all G cones, we used a cocktail of digoxigenin-labelled riboprobes against the four medium-wavelength-sensitive opsins of zebrafish (*opn1mw1, opn1mw2, opn1mw3*, and *opn1mw4*, accession Nos. AF109369, AB087806, AB087807, and AF109370, ZFin ID: ZDB-GENE-990604-42, ZDB-GENE-030728-5, ZDB-GENE-030728-6, and ZDB-GENE-990604-43, respectively). Fluorescein-labelled riboprobes against the blue-sensitive opsin (*opn1sw2*, accession No. AF109372, ZDB-GENE-990604-40) was synthesized as previously described (Barthel and Raymond, 2000). To ensure detection of all R cones, we applied a cocktail of riboprobes against both long-wavelength-sensitive opsins (*opn1lw1* and *opn1lw2*, accession Nos. AF109371 and AB087804, ZDB-GENE-990604-41 and ZDB-GENE-040718-141, respectively) labelled with dinitrophenol. Dinitrophenol-labelled riboprobes were synthesized using unlabelled ribonucleotides (Roche Diagnostics, Indianapolis, IN; No. 11-277057-001) in an in vitro transcription reaction, and these riboprobes were then covalently linked to dinitrophenol using a kit (Mirus Corporation, Madison, WI; No. MIR 3800) as per the manufacturer's instructions. Full-length antisense riboprobes (varying in length; see accession Nos.) were synthesized from linearized plasmid in each case. Each of these seven individually synthesized riboprobes has been used in previously published studies (Barthel and Raymond, 2000; Raymond and Barthel, 2004; Takechi and Kawamura, 2005); they were mixed into a cocktail and applied in

excess to larval fish or isolated adult retinas as described previously (Barthel and Raymond, 2000), except that hybridization temperatures and posthybridization washes were at 65°C. Riboprobes were detected serially using antidigoxigenin (antibody produced by direct immunization of digoxigenin into sheep; then, ion-exchange chromatography and immunoabsorption were used to isolate IgG; Roche Diagnostics; No. 11207733910), antifluorescein (antibody produced by direct immunization of fluoroscein into sheep; then, ion-exchange chromatography and immunoabsorption were used to isolate IgG; Roche Diagnostics; No. 11426346910), or antidinitrophenol (Perkin-Elmer; No. NEL747A001KT) antibodies conjugated to peroxidase. These antibodies failed to label cone photoreceptors specifically if riboprobes were not applied during hybridizations (data not shown). After application of the antibody as described previously (Barthel and Raymond, 2000), the tissue was incubated in tyramide conjugated to AlexaFluor 350, 568, or 647 (Invitrogen; No. T20917, T20914, or T20926) or conjugated to biotin (Perkin-Elmer; No. NEL700) as per manufacturer's protocols. The latter was detected with streptadvidin-conjugated AlexaFluor405 (Invitrogen; No. S32351). After development of each fluorescent signal, the antibody was deactivated by incubating the tissue in 1.5% H_2O_2 for 30 minutes at room temperature. After several washes with PBS-TTD, the tissue was processed with the next antibody and the appropriate tyramide-conjugated-fluorochrome. Variations in the order of the fluorescent detection did not produce noticeably different results. Application of full-length sense riboprobes failed to produce any specific signals. After in situ hybridization and visualization of all signals, the GFP within UV-sensitive cones was detected by using immunocytochemistry with rabbit anti-GFP (1:500; IgG fraction of antibody raised against GFP isolated directly from *Aequorea victoria*; Invitrogen; No. A11122) and anti-rabbit AlexaFluor488 (1:1,000; Invitrogen; No. A21441). These antibodies failed to label the retina in animal without the GFP transgene (data not shown). Images were collected on a Zeiss Axio Image.Z1 Epifluorescent Microscope (Carl Zeiss Microimaging Inc., Thornwood, NY), including the Mosaix function to collect multiple high-magnification images for reconstruction into an image of the entire retina. All images presented are from a single focal plane, except for Figure 6, which stitches together multiple images collected at several focal planes.

Image manipulation and identifying centers of cones

To determine the relative positions of each cone class, we found that semiautomated detection of fluorescent signal was adequate for the UV- and blue-sensitive cones. Here we utilized thresholding functions in Zeiss AxioVision software (release 4.5) to outline the fluorescent signal from either of the cone subtypes, with some adjustments by hand, and recorded the x–y coordinates of the center of each cone as determined by the Zeiss AxioVision software function. For the R and G cones, we found that the thresholding functions were not as reliable for representing cone positions; this likely is due to anatomical features of the R and G cones (elongated apical–basal axis) and their higher density, which sometimes resulted in a lack of physical separation between the signals from individual cells when viewed in flat-mount preparations. Thus we outlined the fluorescent signal from R and G cone opsin by hand with a digitizing tablet (Intuos2 Graphics Tablet; Wacom Ltd., Tokyo, Japan; model No. XD-0912-U) and recorded the x–y coordinates of the centers of the profiles. We note that these methods do not necessarily determine the morphological centers of the cone profiles but rather determine the centers of the opsin mRNA or GFP localization. The localization of green-sensitive opsin mRNA is particularly asymmetric, as discussed below. The x–y coordinates of the geometric centers of the cone opsin mRNA profiles were plotted (Microsoft Excel) for visualization. Images were merged in Axioimager such that the fluorescent signals representing red-, green-, blue-, and UV-sensitive opsins were pseudocolored red, green, cyan, and magenta, respectively. Images presented were merged, cropped, pseudocolored, and adjusted for brightness and contrast in Zeiss AxioVision software (Release 4.5) and/or Adobe Photoshop CS3 10.0.1.

Statistical analysis of cone patterns

To quantify the patterns of distribution of cone photoreceptors, we calculated several indices. These included the ratio of each cone subtype relative to other cone subtypes in a given retinal area. For this purpose, we counted the number of labelled cones and used heterogeneity χ^2 tests to compare the ratio of cones to the expected frequencies in the canonical zebrafish row mosaic: an equal number of R and G cones, an equal number of UV and B cones, and twice as many R or G compared with B or UV. To analyze the homotypic regularity of cones, i.e., the regularity in spacing of one cone subtype relative to others of the same subtype, we used the x–y coordinates of the centers of the cone opsin signals. Heterotypic regularity of cones, i.e., the regularity in spacing of one cone subtype in relationship to another subtype, was similarly calculated using the Pythagorean distance between the centers of two cones of different types. Mean nearest-neighbor distances of cones were determined and conformity ratios were calculated (Cameron and Carney, 2000; Cook and Chalupa, 2000) to assess the amount of

variance in cone spacing. Statistical significance of the conformity ratio as a measure of regularity of cone spacing was determined as recommended by Cook (1996). The individual conformity ratios and cone ratios from multiple images were then compared by Kruskal-Wallis analysis of variance by ranks test calculated in SPSS (SAS, Chicago, IL).

We also developed a novel index of local cone pattern that we have termed a "mosaic metric." We reasoned that local variations in the heterotypic mosaic pattern would change the identity of the cone neighbors. We chose to assess the identity of the cones nearest to a given B cone, reiterate the process for every B cone in a sample, and report the averages of the neighboring cone subtypes in a given retinal region. For example, in considering the schematic of the row mosaic in Figure 1, one expects that the eight closest neighbors to any B cone would consist of two UV cones, two R cones, four G cones, and zero B cones. Because of sample availability, our analysis focused on triple-labelled material; R cones were not labelled, and we noted the identity of the six cones closest to each B cone, expecting them to include two UV cones, four G cones, and zero B cones. To perform this calculation, we created algorithms in MatLab (The MathWorks, Natick, MA) that 1) calculated the Pythagorean distance between the center of a given B cone and the center of every other cone in the array, 2) ranked these distances to calculate which were the six nearest cones, 3) reported the identity of these six cones in terms of cone opsin expression, 4) reiterated steps 1–3 for every B cone in the sample, and 5) calculated the mean number of each neighbor subtype for a given region. These means were expressed as ratios and compared to the expected values using a χ^2 test as calculated in SPSS.

The terminology used to describe the types of cone photoreceptor patterns observed includes larval, larval remnant, and adult. Larval specimens examined were intact eyes from fish 3–4 dpf in age. Specimens from adults were isolated retinas, and we delineated the retinal region surrounding the optic disc, which was generated during larval development, from the remainder of the retina, which was generated by cell addition during postlarval growth. The former we denote as the "larval remnant," and the latter as "adult" retina.

RESULTS

Multiplex in situ hybridization of opsins is effective for analysis of cone patterns

To understand how the heterotypic mosaic of cells is patterned, we first developed methods based on a combination of histological, in situ hybridization, and immunocytochemical analysis to identify multiple cone subtypes in a single retinal preparation and to analyze their local spatial relationships. We assessed our methods in adult zebrafish cone mosaics, in which a canonical "row mosaic" is known to be present (Fig. 1). To reveal the complete mosaic pattern, we used in situ hybridization labelling of opsins for three cone subtypes (blue-, green-, and red-sensitive opsins) in retinas from transgenic fish that express GFP in the UV-sensitive cones (Fig. 2). This image is representative of the labelling throughout the adult zebrafish retina in locations that develop in postlarval stages of fish life, i.e., regions that are not adjacent to the optic nerve head. Rows of single B and UV cones alternating with rows of double R and G cones radiate outward from the posterior pole, and, to accommodate the increasing circumference, additional cone rows are periodically added, creating Y-junctions (Nishiwaki et al., 1997). Multiple opsin subtypes were not detected within individual cone photoreceptors, and the similarity of the labelling pattern to the canonical row mosaic pattern further confirms the specificity of each of these riboprobes (Barthel and Raymond, 2000; Raymond and Barthel, 2004; Takechi and Kawamura, 2005).

We plotted the positions of each of the cone spectral subtypes to reveal their spatial patterns (Fig. 2C). The resemblance of this pattern to the schematic version of the canonical row mosaic is apparent (compare Figs. 1 and 2C). The labeling strategy used in the multiplex preparation shown in Figure 2 to plot positions of individual cones and to identify their subtypes employed the GFP transgene; a reporter that fills the cytoplasm of UV cones; and triple in situ hybridization for the red, green, and blue opsin riboprobes. Because UV and B single cones are discrete, and their apical–basal axis is orthogonal to the retinal surface, in retinal flat mounts the fluorescent signals from reporter and riboprobe, respectively, are nearly solid circular profiles that accurately represent the relative positions of these cone subtypes in the planar mosaic array (Fig. 2B). However, because R and G cone pairs are elongated in their apical–basal axis, twisted together, and fused along their inner segment/myoid region where the opsin mRNA is localized (Raymond et al., 1993), in retinal flat mounts the fluorescent signals from these cone subtypes appear as asymmetric crescents; the signals from the green opsin riboprobe are particularly skewed (Fig. 2D). Therefore, the x–y coordinates of the centers of the red and green opsin profiles, which were used to define the positions of the R and G cones shown in the image in Figure 2C, do not accurately represent the spacing between R and G cones. In reality, pairs of R and G double cones are tightly apposed (in the vertical axis in Fig. 2C), and the apparent space between them (which appears as horizontal black rows in Fig. 2C) is an unavoidable artifact of the labeling method.

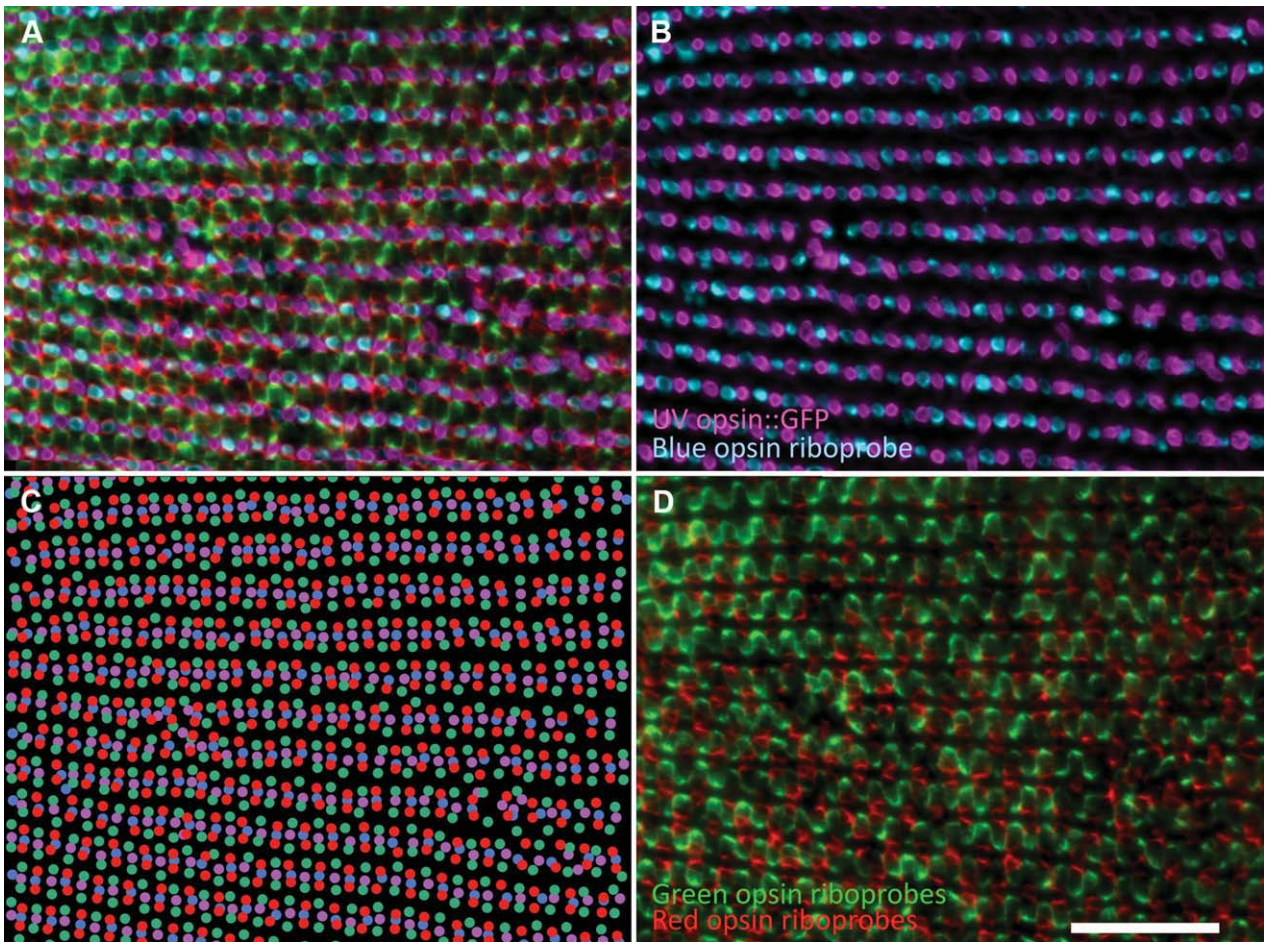

Figure 2. Cone photoreceptor subtype positions in a retina from an adult zebrafish determined by markers for opsin expression. **A**: Triple-label multiplex in situ hybridization with riboprobes against blue-, green-, and red-sensitive opsins on a transgenic retina expressing GFP in UV-sensitive cones. Fluorescent signals are pseudocolored cyan, green, red, and magenta, respectively. **B** is the same field as A with only UV and B channels; **D** is the same field as A with only the G and R channels. **C**: Reconstruction of experimental data presented in A in which circles representing each of the four spectral subtypes are centered on the x–y coordinates of each cone profile identified in the digitized images of the four fluorescent signals (for details see Materials and Methods). The central retina (i.e., optic nerve head) is to the left in this image, and the retinal periphery is to the right, such that the rows of cones are slightly farther apart toward the periphery. D is replicated as Supporting Information Figure 1 in magenta-green. Scale bar = 50 μm. [Color figure can be viewed in the online issue, which is available at wileyonlinelibrary.com.]

Note the reiterated mirror symmetry of the cone mosaic pattern in the direction orthogonal to the rows of double and single cones: B cones are flanked by R cones, and UV cones are flanked by G cones. The ratios of cone subtypes in various retinal areas (dorsal, ventral, temporal, nasal) of adult fish, excluding the region near the optic nerve head, are not significantly different from the expected ratios of 1:1 for R:G or U:B and 2:1 for R or G:B or UV (Table 1, Fig. 3).

Larval cone photoreceptors have heterotypic mosaic patterns but lack the canonical row mosaic of adults

In multiplex preparations of whole-mount larval zebrafish retinas, the canonical row mosaic described in Figure 1 is not apparent (Fig. 4). We first examined the homotypic mosaic patterns for each spectral subtype in the larval retina by analyzing the conformity ratios, a ratio of the average nearest-neighbor distance to the standard deviation. The values of conformity ratios obtained for the various cone subtypes measured in larvae (Table 2) indicate that the spacing of each cone subtype is highly regular (i.e., significantly different from a random or clumped distribution). Notably, the conformity ratios of the UV cones were significantly lower in the larvae compared with adults ($P = 0.002$) as determined by Kruskal-Wallis analysis of variance. Thus homotypic cone relationships are highly regular in zebrafish larvae but not as regular as in the adult.

We next asked whether the ratio of cone subtypes in larval retinas was the same as in the adult, and we found that it was not. We counted the number of each cone

TABLE 1.

Cone Photoreceptor Occurrence in Zebrafish Retina Comparing Cone Subtype Ratios in Various Areas and Developmental Stages With Expected Cone Distributions

		Retinal area		
Cone ratios[1]	Expected[2]	Adult	Larvae	Larval remnant in adult
U:B	1.0	0.83 ± 0.22 (22)	1.15 ± 0.24 (11)	0.35 ± 0.21 (4)
U:G	0.5	0.49 ± 0.08 (17)	0.87 ± 0.22 (11)	0.64 (1)
U:R	0.5	0.31 ± 0.20 (4)	0.87 ± 0.36 (4)	0.15 ± 0.36 (3)
B:R	0.5	0.47 ± 0.04 (4)	0.66 ± 0.11 (12)	0.54 ± 0.11 (3)
B:G	0.5	0.54 ± 0.06 (17)	0.83 ± 0.15 (19)	1.08 (1)
R:G	1.0	0.99 ± 0.06 (3)	1.27 ± 0.27 (13)	nd

[1]Cone names abbreviated U, B, G, and R refer to ultraviolet-, blue-, green-, and red-sensitive cones, respectively. Results for cone ratios ± standard deviation. Within parentheses are the numbers of larvae sampled or number of regions examined in adults. nd, Not determined.
[2]Based on schematic representations and histology of adult fish; see text and Figure 1.

subtype in whole-mount preparations with two, three, or four cone subtypes labeled and found that the ratios are significantly different from ratios in adult retinas ($P < 0.001$) and from the expected ratio in the row mosaic ($P < 0.02$), and the variances of the larval cone ratios are greater (Table 1, Fig. 3). Compared with the expected or adult retina, the larval retinas have an excess of UV cones relative to all other subtypes and an excess of B cones relative to R and G cones.

The mosaic metric tool also revealed a difference between larvae and adults (Fig. 5) that is consistent with an excess of UV cones in larvae. We assessed the fidelity of the mosaic metric tool by applying it to adult fish: this produced numbers that are not significantly different from expected (χ^2, $P > 0.25$; 17 images from n = 3 fish). In larval fish (4 dpf), the local order of cones assessed by the mosaic metric was significantly different from expected (χ^2, $P < 0.025$; six images from six fish). The mosaic metric data from larvae were also significantly different from adult data (under the assumption in the statistical test that the mean of the data from adults is the expected ratio).

Despite the lack of a regular row pattern in the larval retina, the arrangement of cone subtypes relative to one another is not random. We assessed the regularity of spacing between heterotypic cones by calculating the conformity ratios of cone subtype pairs (Table 2). Larval heterotypic conformity ratios (higher numbers indicating regularity) are significantly different from random, toward regularity, regardless of cone types being compared. We further assessed the regularity of the larval cone mosaic by adapting our mosaic metric algorithm to report the identity of the nearest neighbor (rather than the six nearest neighbors; see above). The identity of the nearest neighbor is not random: the nearest neighbor to a G cone in larval retina is typically an R cone (71.0% ± 10.6, n = 8; R, G, and B cone positions considered), whereas in a random distribution of neighbors it would conservatively be expected to be less than 40%. The regularity of the cone mosaic in larval retinas is also observable based on the small variance between samples (Fig. 5). Thus the larval cone mosaic of zebrafish does not have the canonical row mosaic, nor are the homotypic mosaics uncorrelated. Instead, the larval cone positions of B cones with respect to UV, R, and G cones all satisfy the definition of a heterotypic mosaic of cells.

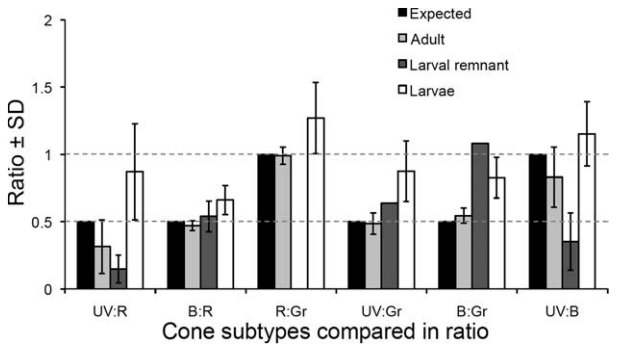

Figure 3. Ratios of cone photoreceptor subtypes in various stages of zebrafish development. The canonical row mosaic of adult zebrafish predicts ratios of cones (black bars and dashed lines; see Fig. 1). The ratios observed in adults are not significantly different from expected (χ^2, $P > 0.05$). Cone ratios in larvae are significantly different from expected (χ^2, $P < 0.03$), with an excess of UV cones relative to other types and an excess of B cones relative to R or G cones compared with that expected from the canonical row mosaic. Cone ratios within the region of retina surrounding the optic nerve head that was generated during larval development (the larval remnant) are also different from expected (χ^2, $P < 0.03$). See also Table 1. Data are represented as ratios ± standard deviation.

Transition to the adult pattern and the larval remnant

We next addressed the timing of the transition between the larval and the adult mosaics. We used cell birth dating to mark the developmental age of cone photoreceptors; we exposed zebrafish larvae to BrdU at 7

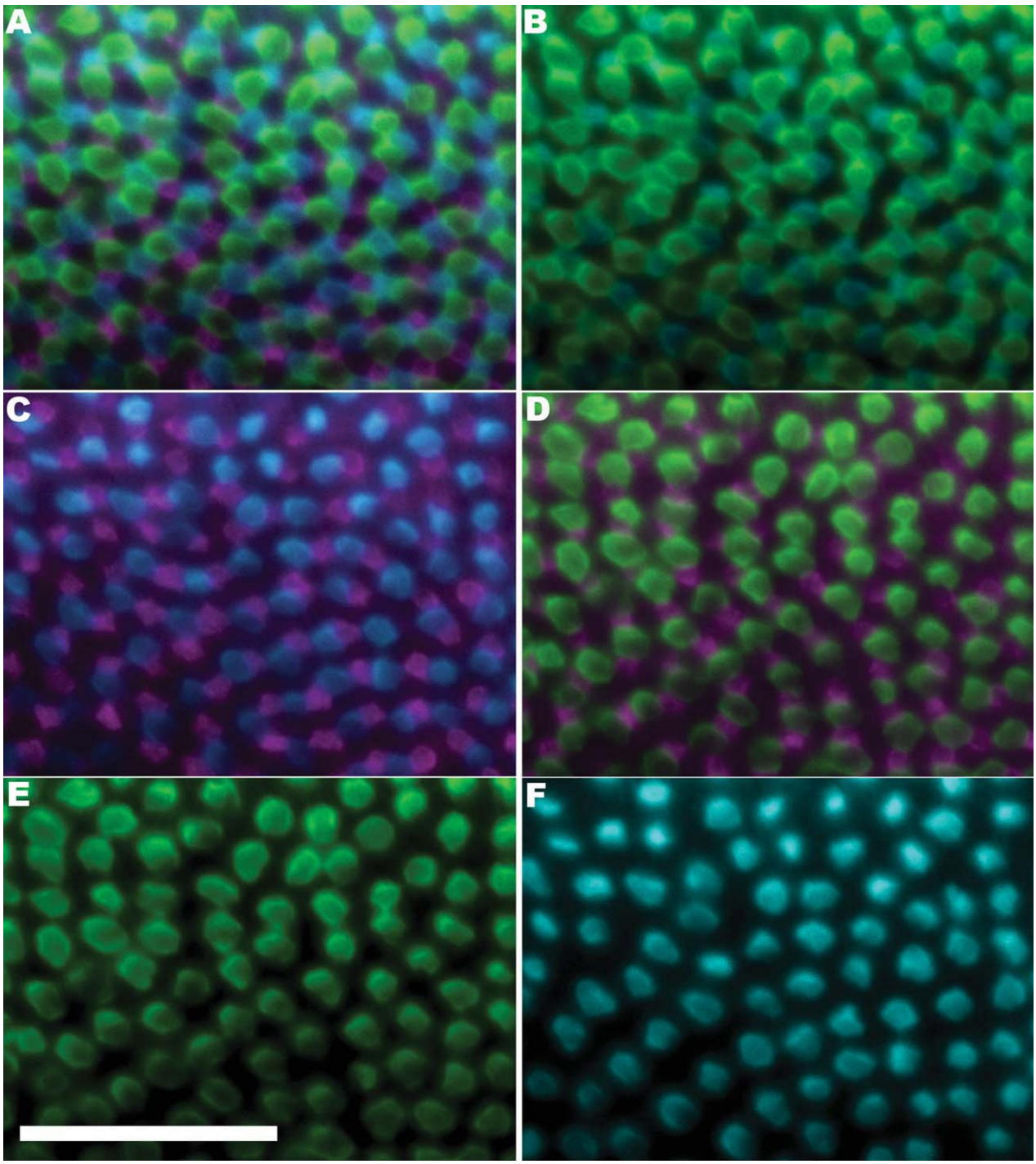

Figure 4. Cone photoreceptor subtype positions in a retina from a larval zebrafish (4 days postfertilization; dpf) determined by markers for opsin expression. **A**: Double-label in situ hybridization using riboprobes against blue- and green-sensitive opsins on a transgenic retina expressing GFP in UV-sensitive cones. Fluorescent signals are pseudocolored cyan, green, and magenta, respectively. The areas not occupied by fluorescent signal can be expected to contain predominantly red-sensitive cones and a few rods (data not shown). B–F are the same field as A, with only subsets of the channels displayed. **B** displays B and G channels; **C** displays UV and B channels; **D** displays UV and G channels; **E** displays the G channel; **F** displays the B channel. Figure 4 is replicated as Supporting Information Figure 2, with the same data represented in magenta-green. Scale bar = 50 μm. [Color figure can be viewed in the online issue, which is available at wileyonlinelibrary.com.]

dpf, allowed the fish to grow for several months, and then prepared retinal flat mounts. Figure 6 demonstrates the pattern of UV cones in a representative example. Inspection of the image reveals regular rows of UV cones throughout most of the retina, with the exception of the region within the ring of BrdU labeling and immediately

TABLE 2.

Regularity of Spacing of Cone Photoreceptor Subtypes in Zebrafish Retina Comparing Various Areas and Developmental Stages

	Retinal area		
Conformity ratio[1]	Adult	Larvae	Larval remnant in adult
U	10.6 ± 0.83 (4)[a]	6.91 ± 0.40 (11)[a]	4.39 ± 1.32 (4)[a]
B	8.10 ± 1.19 (5)[a]	5.19 ± 1.79 (6)[a]	4.39 (1)[a]
G	6.47 ± 0.73 (6)[a]	5.19 ± 1.94 (4)[a]	6.22 (1)[a]
R	6.96 (1)[a]	5.38 ± 1.67 (5)[a]	2.52 ± 1.40 (2)[a,e]
U→B	4.04 ± 1.18 (5)[a]	3.56 ± 0.78 (6)[5a,1c]	3.28 ± 0.30 (2)[a,d]
B→U	3.23 ± 1.12 (5)[a]	2.83 ± 0.62 (6)[3a,3d]	1.93 ± 0.29 (2)[c,d]
U→G	3.05 ± 0.69 (4)[a]	3.35 ± 0.75 (6)[5a,1e]	4.48 (1)[a]
B→R	4.40 (1)[a]	3.22 ± 0.59 (5)[a]	2.45 (1)[c]
B→G	4.13 ± 0.72 (4)[a]	3.97 ± 0.62 (6)[a]	nd

[1]Data presented as mean of conformity ratios for multiple samples and the standard deviation around this mean. Numbers in parentheses represent the numbers of fish sampled. Conformity ratio is a measure of the regularity of cone spacing within each sample (nearest-neighbor distance/standard deviation), with higher ratios indicating more regularity. When a single cone type is listed, homotypic conformity ratios are reported. When two cone types are listed, the distance from each of the first cone subtype to the nearest neighbor of the second subtype was calculated. Cone names abbreviated U, B, G, and R refer to ultraviolet-, blue-, green-, and red-sensitive cones, respectively. nd, Not determined. Significant nonrandomness of cone spacing toward regularity is indicated as $^{a}P < 0.0001$, $^{b}P < 0.001$, $^{c}P < 0.01$, $^{d}P < 0.05$, $^{e}P > 0.05$ (not significant). When one superscript is listed, each individual fish met this significance criterion. When multiple subscripts are listed, this represents significance for different individual fish. When a superscript is preceded by a number, this represents the number of fish in the treatment that reached this level of significance.

adjacent to it. Conformity ratios of UV cone spacing (Table 2) confirm that the distribution of UV cones in this "larval remnant" within the BrdU ring is significantly less regular ($P < 0.001$) than in more peripheral regions but is not different from that in the larval retina ($P = 0.112$). To determine when the row mosaic appears, we applied thymidine analogues BrdU or IdU at different developmental stages. We exposed fish near the end of larval development (20 dpf) to BrdU and then to IdU at 36 dpf (Fig. 7, and data not shown). The larval stage in zebrafish is complete at approximately 3 weeks postfertilization, depending on the characters used in its definition (Brown, 1997; Parichy and Turner, 2003). The row mosaic pattern becomes apparent between the BrdU and the IdU rings in Figure 7, which suggests that cones generated in the postlarval retina become organized into rows. Note that the application of IdU appears to have transiently caused a loss of UV cones; gaps in the regular array occur in and immediately peripheral to the IdU ring (Fig. 7D). Although we are uncertain of the reason for this disruption, it may be a result of toxicity of the IdU label. Regardless, this does not affect our conclusion that UV cones had become regularly patterned prior to IdU application.

The results from the BrdU/IdU labeling (Fig. 7) also confirm that the region surrounding the optic disc that lacks a row mosaic pattern was generated during larval development and is therefore correctly designated as the "larval remnant." However, analysis of cone ratios (Fig. 3) and mosaic metric values (Table 1, Fig. 5) in the larval remnant reveals some differences compared with larval retina. The larval remnant has a lower ratio of UV cones compared with R (Table 1, $P = 0.011$) or B (Table 1, $P = 0.034$) cones as determined by Kruskal-Wallis analysis of variance by ranks. This decreased abundance of UV cones is reflected in a reduction in the number of nearest-neighbor UV cones in the mosaic metric (Fig. 5). Further analysis with additional samples is required to characterize more fully the postlarval changes in the cone ratios and patterns in the larval remnant.

DISCUSSION

For this morphometric, quantitative analysis of the spatiotemporal pattern of the cone mosaic in zebrafish, we used three separate indices of cone pattern. 1) The conformity ratio measures the local regularity of spacing of the mosaic pattern for a given spectral cone subtype(s); this index showed that cones in larvae are regularly spaced (see also Raymond and Barthel, 2004) but not as regularly as in adults. 2) Ratios of cone spectral subtypes confirmed that the cone mosaic of larvae is different from that of adults. 3) We developed a novel "mosaic metric" algorithm to assess local and second-order cone spacing; this measure further confirmed our overall findings.

We offer the following general conclusions. 1) The cone photoreceptors in zebrafish larvae have a heterotypic mosaic array but lack the row mosaic pattern characteristic of the adult retina. 2) The ratio of cone spectral subtypes in the larval retina is different from the adult ratio; adults possess equal numbers of R and G cones, equal numbers of B and UV cones, and twice as many R and G as B and UV; larvae have an excess of UV cones and a smaller excess of B cones. 3) The cones generated in the larval retina do not reorganize into a row mosaic pattern as the

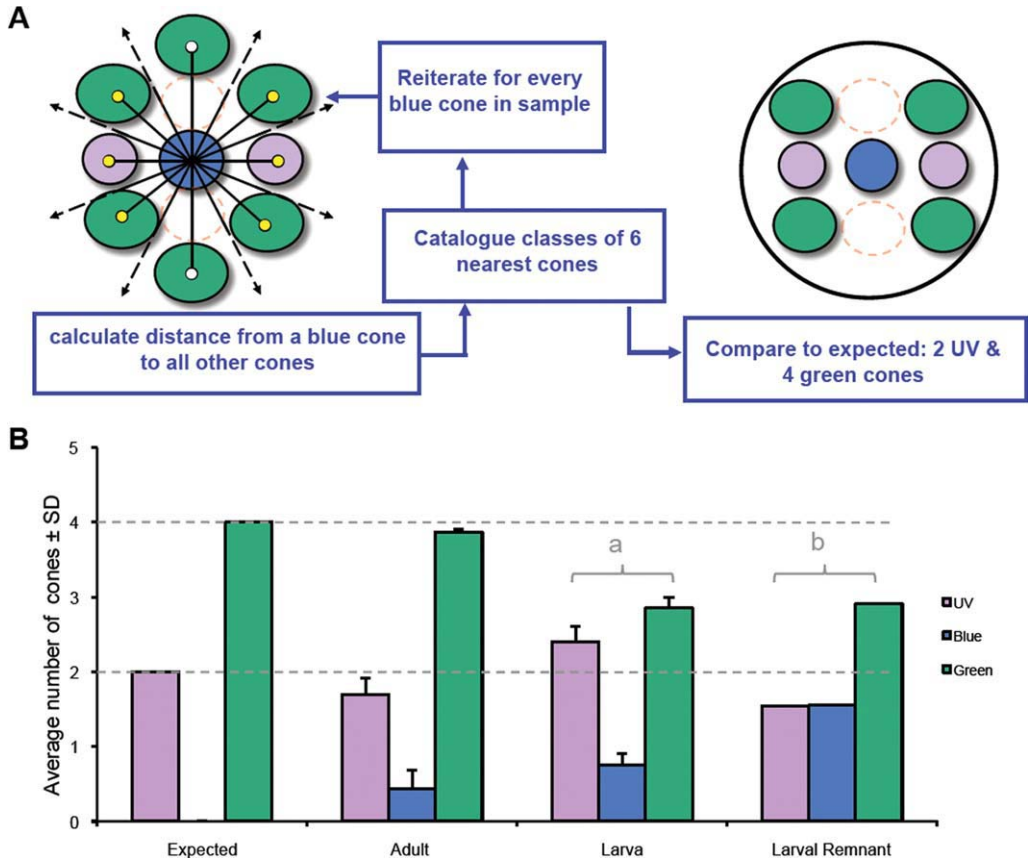

Figure 5. The mosaic metric index reveals local cone patterns in adult retinas consistent with the canonical row pattern, whereas larval retinas show more variability. **A**: The mosaic metric catalogues the identity of the six cones closest to each B cone in the sample by first finding the distance from a B cone to every other labeled cone (lines with white circles or arrowheads) and identifying the six closest cones (yellow circles). This algorithm is then reiterated for every B cone, and data are compiled for comparison with expected values. The samples are labelled for B, UV, and G cones only, so R cones are represented by dashed circles and were not included in the analysis. For the canonical row mosaic, we expect the result to be two UV cones, zero B cones, and four G cones. **B**: Mosaic metric analysis. Cone patterns in adult retinas are not significantly different from expected (χ^2, $P > 0.25$; 17 images from n = 3 fish). Cone patterns in a larval retina are significantly different from expected (χ^2, $P < 0.025$, n = 6 fish; labeled "a"). Cone patterns in a remnant of larval retina retained in the adult (n = 149 blue cones in one retina) are also significantly different from expected (χ^2, $P < 0.0001$, labeled "b"), although the nature of the difference is distinct in the larvae and larval remnant. Dashed lines note expected values, which are also indicated at the left side of the graph. [Color figure can be viewed in the online issue, which is available at wileyonlinelibrary.com.]

retina continues to grow; although some remodeling of this larval mosaic may occur, a "larval remnant" that lacks the row mosaic can be identified adjacent to the optic nerve head in the adult retina. 4) The ontogenetic transition of zebrafish cone photoreceptors into the precise organization of the row mosaic provides baseline data for understanding the formation and refinement of heterotypic mosaics. 5) The ontogeny of the canonical row mosaic is approximately coincident with a metamorphic transition and may be associated with new visually mediated tasks.

The absence of the canonical row cone mosaic had not previously been noted in larval zebrafish retina. This new observation raises the intriguing question of how the organization of larval cones might be transformed into the canonical, famously precise pattern of the adult zebrafish retina. One possible mechanism for refining the cone mosaic pattern is cell death, a process that is known to model cone mosaics of developing salmonids (Allison et al., 2006); cell death has also been reported in the larval zebrafish retina (Biehlmaier et al., 2001). Another mechanism might be cell movements, especially occurring in concert with cell death. Cell movements have been shown to play a role in forming heterotypic mosaics in other systems (Eglen, 2006). However, our analysis showed that remodeling of the larval cone mosaic pattern by cell death or cell movement is not required, insofar as the precise row mosaic pattern of the adult retina is generated entirely by postlarval growth, and the larval mosaic pattern persists in the retina of the adult fish as a remnant surrounding the optic disc. Our analysis has not

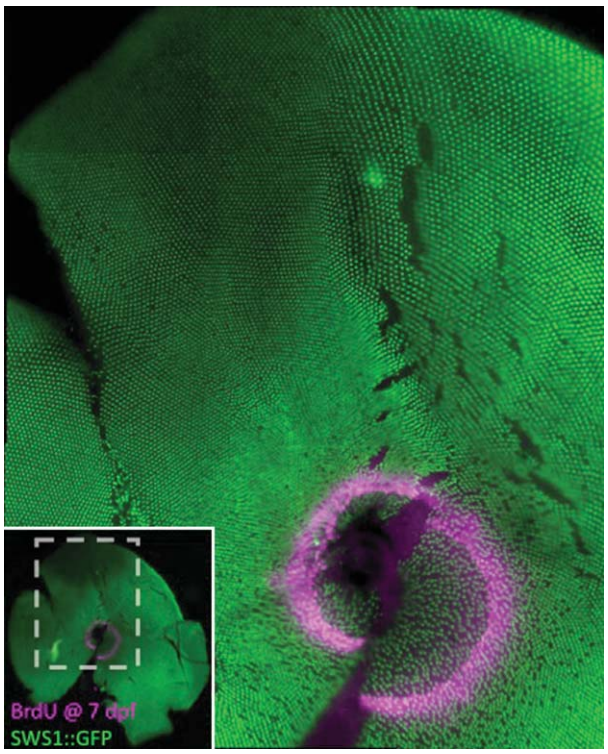

Figure 6. Flat-mounted preparation of adult retina demonstrates that the cone pattern present in the larval zebrafish is retained as a "larval remnant," i.e., a relatively disorganized region of cone mosaic. This transgenic zebrafish (UV cones labeled with GFP) was treated with BrdU at 7 dpf and killed when 3 months old. Note the absence of a row pattern of UV cones within and immediately adjacent to the ring of BrdU. **Inset** shows location of the main image (boxed area) within the entire retinal flat mount. [Color figure can be viewed in the online issue, which is available at wileyonlinelibrary.com.]

excluded cell death and cell movements as potential mechanisms shaping the cone mosaic pattern; indeed, our data suggest that differential loss of UV cones or other remodeling might occur in the larval remnant. It remains to be determined whether a larval remnant of cone mosaic pattern exists in other teleost species.

Previous studies have identified two phases of cone photoreceptor differentiation during zebrafish ontogeny. The first phase is a wave of cone photoreceptor differentiation that sweeps around the retina from the initial site of differentiation, which is confined to a small ventral patch (Hu and Easter, 1999; Raymond and Barthel, 2004). The second phase involves retinal growth by addition of new cone photoreceptors, and other retinal neurons, at the periphery (Hu and Easter, 1999; Raymond and Barthel, 2004; Raymond and Hitchcock, 2004). We have now identified a third phase of cone differentiation in zebrafish, in which the positioning and choice of cell fate of newly generated cones assumes a greater level of precision. An unanswered but intriguing question is whether a correct ratio of cone subtypes (two red:two green:one blue:one UV) is sufficient to produce the canonical row mosaic or perhaps is not sufficient but is necessary in combination with other factors such as differential cell adhesion (Mochizuki, 2002; Podgorski et al., 2007). Our analysis provides a quantitative, statistical description of cone mosaic order that will allow such hypotheses to be tested by mathematical modeling and biological experimentation.

The remodeling of mosaic arrangements of cone subtypes during ontogeny has been noted in the context of a switch between canonical row and square cone mosaic in some teleost fish species (Ahlbert, 1969; Lyall, 1957; Malicki, 1999; Wan and Stenkamp, 2000) or changes in the patterns in other types of mosaic (Beaudet et al., 1993). Movements of individual cones have also also been associated with circadian rhythms in retinal function (Wahl, 1994). The functional significance of these rearrangements in cone positions, whether transient or developmental, is unclear, as are the visual consequences of the precise arrangement and positioning of cone subtypes. Speculations on the underlying developmental mechanisms that pattern the cone mosaic are mostly limited to mathematical modeling (Cameron and Carney, 2004; Mochizuki, 2002).

With regard to the visual ecology of the zebrafish, the transition from a less well-organized larval mosaic, which has moderate homotypic and heterotypic regularity of cone subtype spacing, to the near-crystalline precision of the adult row mosaic of cone photoreceptor subtypes is coincident with the end of metamorphosis, with the resultant changes in fin morphology and body pigmentation (Brown, 1997; Parichy and Turner, 2003). In several other fish species, dramatic changes in life history stages, accompanied by changes in the photic environment and visual tasks, are associated with changes in opsin abundance (Carleton et al., 2008; Spady et al., 2006; Veldhoen et al., 2006) and/or the abundance of cone photoreceptor subtypes (Allison et al., 2006; Mader and Cameron, 2004; Shand et al., 1999, 2008). Thus we speculate that changes in zebrafish cone photoreceptor patterning are associated with changes in visually mediated tasks involving feeding or interacting with conspecifics. These could involve development of mobility related to fin morphogenesis and/or detection of conspecifics associated with changes in pigmentation. Indeed, the increased order in cone mosaic pattern reported here is coincident with an increased preference for visually mediated shoaling behavior (Engeszer et al., 2007). The apparent excess of UV and B cones mediating increased short-wavelength sensitivity in larval zebrafish may be adaptive despite being incompatible with a canonical row mosaic. The timing of the ontogenetic switch

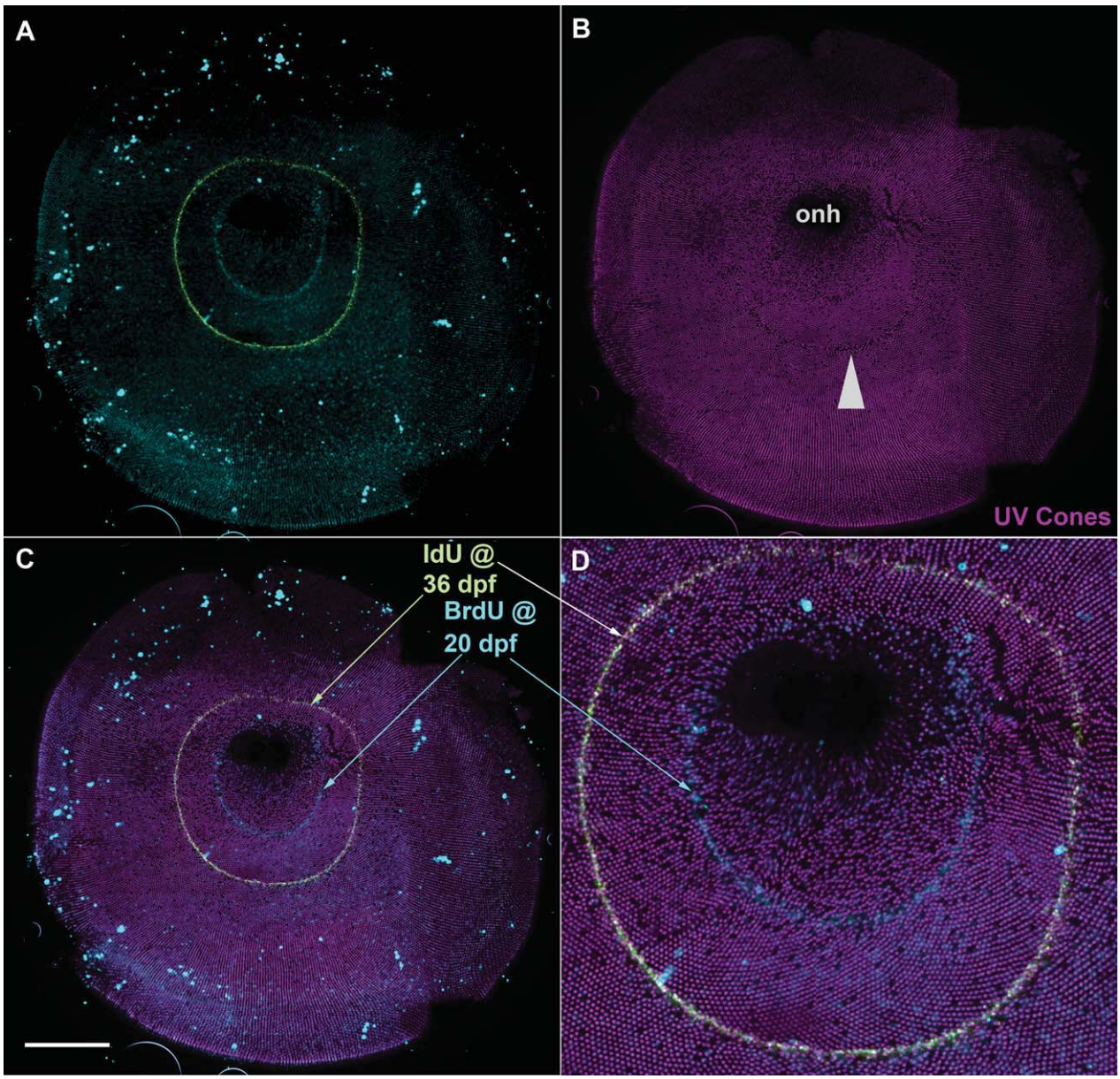

Figure 7. Flat-mounted retinal preparation demonstrates that the row pattern appears in retina generated after larval stages. This transgenic zebrafish (UV cones labeled with GFP, pseudocolored magenta) was treated with BrdU at 20 dpf and IdU at 36 dpf and killed when 8 months old. **A**: Rings of BrdU (blue) or IdU (yellowish green) mark the extent of the retina at the time of treatment; the retina within the BrdU ring was generated when the fish was younger than 20 dpf and includes the optic nerve head (onh). **B**: UV cones expressing GFP (pseudocolored magenta) are aligned in regular rows throughout most of the retina. **C**: Merge of UV cone and thymidine analogues reveals timing of change in cone pattern. **D**: Higher magnification view. UV cones begin to be patterned into rows between the BrdU and the IdU rings. The pattern of UV cones was transiently disrupted by IdU treatment (arrowhead in B); however, it is apparent that the cones were patterned prior to this (D). Scale bar = 500 μm. [Color figure can be viewed in the online issue, which is available at wileyonlinelibrary.com.]

to the row mosaic is also coincident with changes in the spatial distribution of expression of the various representatives of the RH2 (green-sensitive; also known as *opn1mw1, opn1mw2, opn1mw3, opn1mw4*) and LWS (red-sensitive; also known as *opn1lw1, opn1lw2*) classes of opsin mRNAs that occur between 2 and 4 weeks of development (Takechi and Kawamura, 2005). Finally, the timing of this ontogenic switch suggests that thyroid hormone (Brown, 1997) or other metamorphic regulators might play a role in regulating cone differentiation and/or patterning. Indeed thyroid signalling plays important roles in photoreceptor patterning and retinal development in diverse vertebrate species (Allison et al., 2006; Applebury et al., 2007; Marsh-Armstrong et al., 1999; Ng et al., 2001; Roberts et al., 2006; Trimarchi et al., 2008), including modulating green-sensitive cone opsin expression in other fish (Temple

et al., 2008) and mediating the visual sensitivity of adult zebrafish (Allison et al., 2004).

It will be of interest in future studies to investigate how the mechanisms of mosaic formation change during development. These mechanisms may include interactions of homotypic cells (including telodendritic interactions), cell migration, cell death, and lateral induction of cell fates (Eglen and Galli-Resta, 2006; Raymond and Barthel, 2004; Stenkamp et al., 1997; Wikler and Rakic, 1991). Mathematical modeling of teleost cone mosaic formation has also been used to argue that differential cell adhesion could allow cone subtypes to adopt specific spatial relationships (Takesue et al., 1998).

In summary, we have identified a novel ontogenetic transition in cone photoreceptor patterning in zebrafish retina. The cone mosaic is an accessible example of an in vivo vertebrate heterotypic cell mosaic that can be assessed with robust cell-specific markers. Combined with the optical transparency, behavioral repertoire, and genetic toolkit for the zebrafish, the current work establishes a model for understanding the formation and refinement of heterotypic cell mosaics as well as both the development and the function of vertebrate cone photoreceptor mosaics.

ACKNOWLEDGMENTS

We thank Dilip Pawar, Aleah McCorry, and Adina Bujold for technical support.

LITERATURE CITED

Adler R, Raymond PA. 2008. Have we achieved a unified model of photoreceptor cell fate specification in vertebrates? Brain Res 1192:134–150.

Ahlbert I. 1969. The organization of the cone cells in the retinae of four teleosts with different feeding habits (*Perca fluviatilis* L., *Lucioperca lucioperca* L., *Acerina cernua* L., and *Coregonus albula* L.). Ark Zool 22:445–481.

Ali MA, Anctil M. 1976. Retinas of fishes: an atlas. Berlin: Springer-Verlag.

Allison WT, Haimberger TJ, Hawryshyn CW, Temple SE. 2004. Visual pigment composition in zebrafish: evidence for a rhodopsin–porphyropsin interchange system. Vis Neurosci 21:945–952.

Allison WT, Dann SG, Veldhoen KM, Hawryshyn CW. 2006. Degeneration and regeneration of ultraviolet cone photoreceptors during development in rainbow trout. J Comp Neurol 499:702–715.

Applebury ML, Farhangfar F, Glosmann M, Hashimoto K, Kage K, Robbins JT, Shibusawa N, Wondisford FE, Zhang H. 2007. Transient expression of thyroid hormone nuclear receptor TRbeta2 sets S opsin patterning during cone photoreceptor genesis. Dev Dyn 236:1203–1212.

Barthel LK, Raymond PA. 2000. In situ hybridization studies of retinal neurons. Methods Enzymol 316:579–590.

Beaudet L, Browman HI, Hawryshyn CW. 1993. Optic nerve response and retinal structure in rainbow trout of different sizes. Vis Res 33:1739–1746.

Biehlmaier O, Neuhauss SC, Kohler K. 2001. Onset and time course of apoptosis in the developing zebrafish retina. Cell Tissue Res 306:199–207.

Brown DD. 1997. The role of thyroid hormone in zebrafish and axolotl development. Proc Natl Acad Sci USA 94: 13011–13016.

Cameron DA. 2002. Mapping absorbance spectra, cone fractions, and neuronal mechanisms to photopic spectral sensitivity in the zebrafish. Vis Neurosci 19:365–372.

Cameron DA, Carney LH. 2000. Cell mosaic patterns in the native and regenerated inner retina of zebrafish: implications for retinal assembly. J Comp Neurol 416:356–367.

Cameron DA, Carney LH. 2004. Cellular patterns in the inner retina of adult zebrafish: quantitative analyses and a computational model of their formation. J Comp Neurol 471:11–25.

Carleton KL, Spady TC, Streelman JT, Kidd MR, McFarland WN, Loew ER. 2008. Visual sensitivities tuned by heterochronic shifts in opsin gene expression. BMC Biol 6:22.

Chinen A, Hamaoka T, Yamada Y, Kawamura S. 2003. Gene duplication and spectral diversification of cone visual pigments of zebrafish. Genetics 163:663–675.

Collin SP. 2008. A web-based archive for topographic maps of retinal cell distribution in vertebrates. Clin Exp Optom 91: 85–95.

Collin SP, Shand J. 2003. Retinal sampling and the visual field in fish. In: Collin SP, Marshall NJ, editors. Sensory processing in Aquatic Environments. New York: Springer-Verlag. p 139–169.

Cook JE. 1996. Spatial properites of retinal mosaics: an empirical evaluation of some existing measures. Vis Neurosci 13:15–30.

Cook JE, Chalupa LM. 2000. Retinal mosaics: new insights into an old concept. Trends Neurosci 23:26–34.

Cook JE, Noden AJ. 1998. Somatic and dendritic mosaics formed by large ganglion cells in the retina of the common house gecko (*Hemidactylus frenatus*). Brain Behav Evol 51: 263–283.

Dunn RF. 1966. Studies on the retina of the gecko *Coleonyx variegatus*. II. The rectilinear visual cell mosaic. J Ultrastruct Res 16:672–684.

Eglen SJ. 2006. Development of regular cellular spacing in the retina: theoretical models. Math Med Biol J IMA 23:79–99.

Eglen SJ, Galli-Resta L. 2006. Retinal Mosaics. In: Sernagor E, Eglen SJ, Harris WA, Wong R, editors. Retinal development. Cambridge: Cambridge University Press. p 193–207.

Eglen SJ, Wong JCT. 2008. Spatial constraints underlying the retinal mosaics of two types of horizontal cells in cat and macaque. Vis Neurosci 25:209–214.

Eglen SJ, Raven MA, Tamrazian E, Reese BE. 2003. Dopaminergic amacrine cells in the inner nuclear layer and ganglion cell layer comprise a single functional retinal mosaic. J Comp Neurol 466:343–355.

Eglen SJ, Lofgreen DD, Raven MA, Reese BE. 2008. Analysis of spatial relationships in three dimensions: tools for the study of nerve cell patterning. BMC Neurosci 9:7.

Engeszer RE, Barbiano LA, Ryan MJ, Parichy DM. 2007. Timing and plasticity of shoaling behaviour in the zebrafish, *Danio rerio*. Anim Behav 74:1269–1275.

Engström K. 1960. Cone types and cone arrangements in the retina of some cyprinids. Acta Zool 41:277–295.

Engström K. 1963. Cone types and cone arrangements in teleost retinae. Acta Zool 44:179–243.

Fuerst PG, Koizumi A, Masland RH, Burgess RW. 2008. Neurite arborization and mosaic spacing in the mouse retina require DSCAM. Nature 451:470–474.

Hu M, Easter SS. 1999. Retinal neurogenesis: the formation of the initial central patch of postmitotic cells. Dev Biol 207:309–321.

Johnson GD, Araujo GM. 1981. A simple method of reducing the fading of immunofluoresence during microscopy. J Immunol Methods 43:439.

Lyall AH. 1957. The growth of the trout retina. Q J Micro Sci 98:101–110.
Mader MM, Cameron DA. 2004. Photoreceptor differentiation during retinal development, growth, and regeneration in a metamorphic vertebrate. J Neurosci 24:11463–11472.
Malicki J. 1999. Development of the retina. In: Detrich HW, Westerfield M, Zon LI, editors. The zebrafish: biology. San Diego: Academic Press. p 253–272.
Marsh-Armstrong N, Huang H, Remo BF, Liu TT, Brown DD. 1999. Asymmetric growth and development of the *Xenopus laevis* retina during metamorphosis is controlled by type III deiodinase. Neuron 24:871–878.
Mochizuki A. 2002. Pattern formation of the cone mosaic in the zebrafish retina: a cell rearrangement model. J Theor Biol 215:345–361.
Nawrocki L, BreMiller R, Streisinger G, Kaplan M. 1985. Larval and adult visual pigments of the zebrafish, *Brachydanio rerio*. Vis Res 25:1569–1576.
Ng L, Hurley JB, Dierks B, Srinivas M, Salto C, Vennstrom B, Reh TA, Forrest D. 2001. A thyroid hormone receptor that is required for the development of green cone photoreceptors. Nat Genet 27:94–98.
Nishiwaki Y, Oishi T, Tokunaga F, Morita T. 1997. Three-dimensional reconstruction of cone arrangement in the spherical surface of the retina in the medaka eyes. Zool Sci 14:795–801.
Parichy DM, Turner JM. 2003. Zebrafish puma mutant decouples pigment pattern and somatic metamorphosis. Dev Biol 256:242–257.
Podgorski GJ, Bansal M, Flann NS. 2007. Regular mosaic pattern development: a study of the interplay between lateral inhibition, apoptosis and differential adhesion. Theor Biol Med Model 4:43.
Raymond PA, Barthel LK. 2004. A moving wave patterns the cone photoreceptor mosaic array in the zebrafish retina. Int J Dev Biol 48:935–945.
Raymond PA, Hitchcock PF. 2004. The teleost retina as a model for developmental and regeneration biology. Zebrafish 1:257–271.
Raymond PA, Barthel LK, Rounsifer ME, Sullivan SA, Knight JK. 1993. Expression of rod and cone visual pigments in goldfish and zebrafish: a rhodopsin-like gene is expressed in cones. Neuron 10:1161–1174.
Raymond PA, Barthel LK, Stenkamp DL. 1996. The zebrafish ultraviolet cone opsin reported previously is expressed in rods. Invest Ophthalmol Vis Sci 37:948–950.
Reese BE, Raven MA, Stagg SB. 2005. Afferents and homotypic neighbors regulate horizontal cell morphology, connectivity, and retinal coverage. J Neurosci 25:2167–2175.
Risner ML, Lemerise E, Vukmanic EV, Moore A. 2006. Behavioral spectral sensitivity of the zebrafish (*Danio rerio*). Vis Res 46:2625–2635.
Roberts MR, Srinivas M, Forrest D, Morreale de Escobar G, Reh TA. 2006. Making the gradient: thyroid hormone regulates cone opsin expression in the developing mouse retina. Proc Natl Acad Sci USA 103:6218–6223.
Robinson J, Schmitt EA, Harosi FI, Reece RJ, Dowling JE. 1993. Zebrafish ultraviolet visual pigment: absorption spectrum, sequence, and localization. Proc Natl Acad Sci USA 90:6009–6012.
Shand J, Archer MA, Collin SP. 1999. Ontogenetic changes in the retinal photoreceptor mosaic in a fish, the black bream, *Acanthopagrus butcheri*. J Comp Neurol 412:203–217.
Shand J, Davies WL, Thomas N, Balmer L, Cowing JA, Pointer M, Carvalho LS, Trezise AEO, Collin SP, Beazley LD, Hunt DM. 2008. The influence of ontogeny and light environment on the expression of visual pigment opsins in the retina of the black bream, *Acanthopagrus butcheri*. J Exp Biol 211:1495–1503.
Spady TC, Parry JW, Robinson PR, Hunt DM, Bowmaker JK, Carleton KL. 2006. Evolution of the cichlid visual palette through ontogenetic subfunctionalization of the opsin gene arrays. Mol Biol Evol 23:1538–1547.
Stenkamp DL, Cameron DA. 2002. Cellular pattern formation in the retina: retinal regeneration as a model system. Mol Vis 8:280–293.
Stenkamp DL, Hisatomi O, Barthel LK, Tokunaga F, Raymond PA. 1996. Temporal expression of rod and cone opsins in embryonic goldfish retina predicts the spatial organization of the cone mosaic. Invest Ophthalmol Vis Sci 37:363–376.
Stenkamp DL, Barthel LK, Raymond PA. 1997. Spatiotemporal coordination of rod and cone photoreceptor differentiation in goldfish retina. J Comp Neurol 382:272–284.
Takechi M, Kawamura S. 2005. Temporal and spatial changes in the expression pattern of multiple red and green subtype opsin genes during zebrafish development. J Exp Biol 208:1337–1345.
Takechi M, Hamaoka T, Kawamura S. 2003. Fluorescence visualization of ultraviolet-sensitive cone photoreceptor development in living zebrafish. FEBS Lett 553:90–94.
Takechi M, Seno S, Kawamura S. 2008. Identification of cis-acting elements repressing blue opsin expression in zebrafish UV cones and pineal cells. J Biol Chem 283: 31625–31632.
Takesue A, Mochizuki A, Iwasa Y. 1998. Cell-differentiation rules that generate regular mosaic patterns: modelling motivated by cone mosaic formation in fish retina. J Theor Biol 194:575–586.
Temple SE, Veldhoen KM, Phelan JT, Veldhoen NJ, Hawryshyn CW. 2008. Ontogenetic changes in photoreceptor opsin gene expression in coho salmon (*Oncorhynchus kisutch*, Walbaum). J Exp Biol 211:3879–3888.
Trimarchi JM, Harpavat S, Billings NA, Cepko CL. 2008. Thyroid hormone components are expressed in three sequential waves during development of the chick retina. BMC Dev Biol 8:101.
Tyler MJ, Cameron DA. 2007. Cellular pattern formation during retinal regeneration: A role for homotypic control of cell fate acquisition. Vis Res 47:501–511.
Vega CJ, Peterson DA. 2005. Stem cell proliferative history in tissue revealed by temporal halogenated thymidine analog discrimination. Nat Methods 2:167–169.
Veldhoen K, Allison WT, Veldhoen N, Anholt BR, Helbing CC, Hawryshyn CW. 2006. Spatio-temporal characterization of retinal opsin gene expression during thyroid hormone-induced and natural development of rainbow trout. Vis Neurosci 23:169–179.
Vihtelic TS, Doro CJ, Hyde DR. 1999. Cloning and characterization of six zebrafish photoreceptor opsin cDNAs and immunolocalization of their corresponding proteins. Vis Neurosci 16:571–585.
Wahl CM. 1994. Periodic cone cell twists in the walleye, Stizostedion vitreum; a new type of retinomotor activity. Vis Res 34:11–18.
Wan J, Stenkamp DL. 2000. Cone mosaic development in the goldfish retina is independent of rod neurogenesis and differentiation. J Comp Neurol 423:227–242.
Westerfield M. 1995. The zebrafish book. Eugene, OR: University of Oregon Press.
Wikler KC, Rakic P. 1991. Relation of an array of early-differentiating cones to the photoreceptor mosaic in the primate retina. Nature 351:397–400.